This is a preprint, the final version is subject to change, of the American Mineralogist (MSA)
Cite as Authors (Year) Title. American Mineralogist, in press.
(DOI will not work until issue is live.) DOI: http://dx.doi.org/10.2138/am-2016-5588CCBY

REVISION 1

OXYGEN ISOTOPE GEOCHEMISTRY OF MAFIC PHENOCRYSTS IN PRIMITIVE MAFIC LAVAS FROM THE SOUTHERNMOST CASCADE RANGE, CALIFORNIA

S. J. Underwood (corresponding author)

Department of Earth Sciences
Montana State University
Bozeman, MT 59717 USA

Childs Geoscience Inc.
1700 West Koch, Suite 6
Bozeman, MT 59715 USA

M. A. Clynne

United States Geological Survey
345 Middlefield Road
Mail Stop 910
Menlo Park, CA 94025 USA

Corresponding author contact information:
E-mail: SandyUnderwood903@hotmail.com
Home phone: (406) 522-3996
Mailing address: 50 Red Cloud Place
Bozeman, MT 59715-8727

Abstract

Previously reported whole rock $\delta^{18}O$ values (5.6–7.8‰) for primitive Quaternary mafic lavas from the southernmost Cascades (SMC) are often elevated (up to 1‰) relative to $\delta^{18}O$ values expected for mafic magmas in equilibrium with mantle peridotite. Olivine, clinopyroxene, and plagioclase crystals were separated from 29 geochemically well-characterized mafic lavas for $\delta^{18}O$ measurements by laser fluorination to assess modification of the mantle sources by ancient and modern subducted components. Oxygen isotope values of olivine phenocrysts in calc-alkaline lavas and contemporaneous high alumina olivine tholeiitic (HAOT) lavas generally exceed depleted mantle olivine values (~4.9–5.3‰). Modern addition of up to 6 wt.% slab-derived fluid from Gorda serpentinized peridotite dehydration (~15‰) or chlorite dehydration (~10‰) within the serpentinized peridotite can provide the ^{18}O enrichment detected in olivine phenocrysts ($\delta^{18}O_{olivine}$ = 5.3–6.3‰) in calc-alkaline mafic lavas, and elevate ^{18}O in overlying mantle lithosphere, as well. Specifically, although HAOT $\delta^{18}O_{olivine}$ values (5.5–5.7‰) may reflect partial melting in heterogeneous ^{18}O enriched mantle source domains that developed during multiple subduction events associated with terrane accretion (e.g. <1 wt.% of ~15‰ materials), an additional ^{18}O enrichment of up to 2 wt.% of 10–15‰ slab-derived hydrous fluids might be accommodated. The calc-alkaline primitive magmas appear to have experienced a continuous range of open system processes, which operate in the mantle and during rapid magma ascent to eruption, and occasionally post quench. Textural relationships and geochemistry of these lava samples are consistent with blends of mafic phenocrysts and degassed melts in varying states of ^{18}O disequilibrium. In lenses of accumulated melt within peridotite near the base of the crust, co-existing olivine and clinopyroxene $\delta^{18}O$ values probably are not at isotopic equilibrium because fluids introduced into the system perturbed the $\delta^{18}O_{melt}$ values. A 'sudden' melt extraction event interrupts ^{18}O equilibration in phenocrysts and poorly mixed melt(s). Rapid

ascent of volatile oversaturated primitive mafic magma through the crust appears to be accompanied by devolatilization and crystallization of anorthite-rich plagioclase with elevated $\delta^{18}O_{plag}$ values. The $(Sr/P)_N$ values for the whole rock geochemistry are consistent with a $^{87}Sr/^{86}Sr$ ~0.7027 slab-derived fluid addition into the infertile peridotite source of magmas, and melt devolatilization is recorded in the mixture of disequilibrium $\delta^{18}O$ values for the constituent phases of lavas. Morbidity of the Gorda Plate as it undergoes intense deformation from the spreading ridge to the trench is likely a key factor to developing the carrying capacity of hydrous fluids and mineral phases in the slab subducting into the SMC mantle.

Keywords

Southernmost Cascade Range Primitive mafic lavas Oxygen isotopes Phenocrysts Laser fluorination Slab-derived hydrous fluids Magma devolatilization

Introduction

Volcanism in the southernmost Cascades (SMC) of northern California occurs on two distinct scales: (1) large volume, long-lived (up to a million years) volcanic centers ranging in composition from basaltic-andesitic to rhyolitic, and (2) small volume, short-lived (one to a few thousand years) basaltic to andesitic shield volcanoes and scoria cones (Guffanti et al. 1996; Hildreth 2007). This latter regional mafic volcanism is sourced primarily from partial melts of variably depleted mantle wedge peridotites (Borg et al. 1997), yet many of the volcanic rocks have whole rock oxygen isotope ratios ($\delta^{18}O_{whole\ rock}$ = 5.6–7.8‰) that are considerably higher than values typically associated with basaltic melts derived from MORB mantle (5.5±0.2‰; Eiler 2001).

Borg (1995) and Borg et al. (1997) attributed the high $\delta^{18}O_{whole\ rock}$ values of more primitive SMC mafic lavas to large amounts of modern slab-derived hydrous fluids added into sub-arc mantle previously contaminated by small amounts of subducted sediment. They resisted ascribing the high $\delta^{18}O$ values to crustal contamination due to the high compatible-element contents of the rocks, which limit the amounts of crust that may be admixed into the magmas, and the lack of correlations between $\delta^{18}O_{whole\ rock}$ values and indices of differentiation. Moreover, Borg et al. (1997, 2000) concluded that crustal contamination is minor, and rejected modification of whole rock oxygen isotopic ratios by secondary processes (e.g. infiltration and exchange with meteoric waters) because the rocks are young and visibly pristine. In contrast, Bacon et al. (1997) argue that mafic and ultramafic crustal components are significant sources of contamination and, in part, are responsible for elevated $\delta^{18}O_{whole\ rock}$ values. The disparity between the Borg et al. (1997) and Bacon et al. (1997) petrogenetic models (i.e. mantle source modification vs. crustal contamination) was the impetus for this study. Previous investigations of

SMC mafic lavas included petrologic and geochemical studies by Clynne (1993), Borg (1995), Bacon et al. (1997), Clynne and Borg (1997) and Borg et al. (1997, 2000, 2002), which produced a large and comprehensive isotopic data set for the rocks, including whole rock values for Sr, Nd, Pb, Hf, Os, and O isotope ratios. A fruitless search for significant crustal contamination sources for the magmas was abandoned because no reasonable contaminant could be added in amounts that would mutually satisfy constraints implicit in the aforementioned geochemical datasets. However, we determined $\delta^{18}O$ values from phenocryst separates of olivine, clinopyroxene and plagioclase from primitive lavas by laser fluorination to investigate the slab-derived fluid contributions from an oxygen isotope perspective. Our results provide some exciting clues for open system processes that accompany ascent of mafic magmas resulting from subduction of a hot, fluid-rich slab.

Background

Tectonic and geologic setting

Arc volcanism in the Cascades results from subduction of the Gorda/Juan de Fuca/Explorer oceanic plates beneath the continental North American plate (Fig. 1a). In the southern part of the arc, the warm, intensely fractured, high-riding northern segment of the Gorda plate is ~6 Ma where it obliquely converges at 36 mm/year under the large accretionary complex at the leading edge of the North American plate (Dziak et al. 2001; Chaytor et al. 2004). Volcanic activity in the SMC arises from arc magmatism at the southern end of the Cascadia subduction zone and asthenospheric upwelling along the margin where the Gorda lithosphere termination creates a slabless window (Trehu et al. 1995; Gulick et al. 2001).

Neogene east-northeast directed crustal extension of the Basin and Range province overlaps the SMC arc axis producing NNW trending normal faults that are a primary control on volcanic

vent locations (Guffanti et al. 1990, 1996). Lithospheric extension is influenced by far field Pacific plate motion, and dextral shear movement in this diffuse transfer zone from the more proximal Walker Lane (Blakely et al. 1997). Outboard faults of the Walker Lane dextral shear zone terminate in splays that cut the northern end of the Sierra Nevada microplate, which underlies at least part of the SMC rear-arc (Hildreth 2007). The Sierra Nevada microplate generates localized transpressional faulting as it moves northwestwardly relative to North America (Miller et al. 2001).

Thick Cenozoic volcanogenic cover in the SMC region likely mantles major Phanerozoic lithotectonic belts that extend northwesterly from the northern Sierra Nevada (Day and Bickford 2004), and southeasterly from belts in the Klamath Mountains (Dickinson 2008). The accreted terranes include island arcs with fringing aprons of volcanogenic sediments and carbonates, ophiolites, peridotites, and subduction mélanges. All terranes are variably tectonically dismembered, and the assemblages are studded with Mesozoic stitching plutons (Dickinson 2008). This terrane collage is expressed in regional gravity structures (Blakely et al. 1997) and exposures of basement rocks can be found in deep canyons southwest of Lassen Volcanic National Park. Surface faults visible outside of the Lassen Volcanic Center are Neogene, and the widespread regional Quaternary mafic (basaltic to andesitic) volcanic rocks erupted from hundreds of aligned vents forming a platform from coalescing lava flows.

SMC mafic lavas

Two geochemically distinct groups of mafic lavas erupted in the southernmost Cascades during the past 7 Ma (Guffanti et al. 1990; Clynne 1993; Bacon et al. 1997; Borg et al. 1997). Low potassium HAOT lavas are present from the arc axis eastward into the rear-arc and are typically erupted from fissure vents and spatter ramparts (Guffanti et al. 1990). Subduction-related,

143 primitive calc-alkaline basaltic to mafic andesitic lavas are present from the forearc to the rear-
144 arc and are typically low volume (< 1 km^3) block lava flows erupted from small monogenetic
145 shield volcanoes or scoria cones (Clynne 1993). Relative to HAOT lavas, calc-alkaline mafic
146 lavas are dominant in both total volume erupted and in number of individual lava flows (Guffanti
147 et al. 1990, 1996; Bacon et al. 1997).

148 SMC primitive mafic lavas are defined by Borg et al. (1997) as HAOT lavas with $Fo_{86–88}$
149 olivine and chromian spinel with Cr# 10–25 (where Cr# = 100[Cr]/([Cr] + [Al])), and calc-
150 alkaline lavas with $Fo_{86–90}$ olivine and chromian spinel with Cr# 25–75. In addition, both
151 primitive lava types have Ni > 100 ppm, Cr > 200 ppm, MgO > 6 wt%, and Mg# > 66 (where
152 Mg# = 100[Mg]/([Mg] + [Fe^{2+}])). Figure 1b is a map of sample locations of the rocks selected
153 for this study. The fosteritic compositions of olivine phenocrysts in primitive lavas from both
154 groups are in equilibrium with mantle peridotite (Clynne and Borg 1997) and have 1225–1275 °C
155 crystallization temperatures, based on olivine calcium concentrations (Clynne, 1993). HAOT
156 magmas are generally hotter than calc-alkaline magmas (Clynne 1993).

157 HAOT lavas erupted in the SMC are similar to mafic tholeiitic lavas associated with the
158 Basin and Range extensional province (Bullen and Clynne 1989; Guffanti et al. 1990; Clynne
159 1993). These comparatively large volume (often > 1 km^3), low viscosity lavas are typically
160 present as thin, pahoehoe flows (Clynne 1993). The HAOT lavas are sparsely phyric (generally
161 <1% phenocrysts) with olivine or plagioclase phenocrysts in holocrystalline groundmasses
162 (Clynne and Borg 1997). The major element signature of the HAOT lavas is ≤ 0.2 wt% K_2O, 17–
163 18 wt% Al_2O_3, 48–50 wt% SiO_2 and FeO*/MgO ratios of 0.9–1.2 (Clynne and Borg 1997;
164 Bacon et al. 1997).

All primitive calc-alkaline lavas are phenocryst-poor (<5%) with olivine as the primary phenocryst phase, or olivine plus spinel. Clinopyroxene (chromian diopside) is present as a phenocryst phase in some calc-alkaline lavas and plagioclase, when present is small, is thought to crystallize during the latter stage of magma ascent (Clynne and Borg 1997; Borg et al. 1997). Groundmass textures range from intergranular to intersertal. Chemically, the calc-alkaline lavas are more oxidized and have higher large ion lithophile element (LILE) and light rare earth element (LREE) contents, lower heavy rare earth element (HREE) contents and depletions in high field strength elements (HFSE) relative to the HAOT lavas (Bacon et al. 1997). Forearc calc-alkaline lavas have the strongest arc geochemical signature, and range from basalts to high-MgO andesites with low abundances of incompatible trace elements, including high field strength elements (Borg et al. 1997). Mafic calc-alkaline rear-arc lavas are restricted to basalts with high concentrations of incompatible trace elements (Clynne and Borg 1997).

Olivine phenocrysts in both HAOT and most calc-alkaline lavas often contain chromian spinel inclusions in equilibrium with the host olivine. Clynne (1993), Borg (1995), and Clynne and Borg (1997) interpreted the general increase in Cr# of the spinel inclusions (and trace element abundances in corresponding lavas) as indications of decreasing fertility of mantle toward the trench. In calc-alkaline lavas, the spinel inclusions formed at ~12 kbar and have variably higher Cr#s (Clynne and Borg 1997). In HAOT lavas, Clynne and Borg (1997) postulated that crystallization of these Al-rich chromian spinel inclusions occurred at ~11 kbar (cf. Bartels et al. 1991), and that the olivine phenocrysts must have formed contemporaneously or nearly so.

Studies of trace element and radiogenic isotopic systematics concluded that the sub-arc mantle beneath the SMC is compositionally and isotopically heterogeneous and may contain

three endmember components (Bullen and Clynne 1990; Clynne 1993; Clynne and Borg 1997; Bacon et al. 1997; Borg et al. 1997, 2000, 2002). These components include: (1) depleted, MORB-like mantle, (2) mantle enriched with subducted materials, and (3) mantle domains from accreted Northern Sierra and Klamath island arc terranes (Bullen and Clynne 1990; Borg et al. 2002). An 'intraplate' component was invoked to model the geochemistry of calc-alkaline mafic lavas with weak Sr enrichments and low HFSE depletions typical of rear-arc magmas (Bacon et al. 1997; Borg et al. 1997).

Analytical techniques

The SMC mafic lavas selected for this study (Table 1) are well-characterized, nearly pristine (see below) rocks previously investigated by Clynne (1993), Bacon et al. (1997), Borg et al. (1997), Clynne and Borg (1997), and Borg et al. (2000, 2002). Dated samples are Quaternary and mostly < 0.5 Ma with a Mg# range from 66 to 82 (Clynne and Borg 1997). Four of the samples (014, 015, 017 and 036) are non-primitive by our definition, but phenocrysts are probably cognate to their magmatic systems. Similarly, samples (020, 032, 034, and 035) with intermediate trace element abundances and radiogenic isotopic ratios between HAOT and CAB (possibly the results of source mixing) are included. For this work, new material was collected from precisely the same field locations as in the earlier studies. Lava samples are from variable positions vertically and laterally in the flows. The petrography evaluation summary can be found in the Appendix, and example micrographs of the olivine, clinopyroxene and plagioclase phenocrysts are shown in Fig. 2.

Oxygen isotope analyses

Olivine, clinopyroxene, and plagioclase phenocryst separates were prepared by hand-picking primarily 500–425 μm (but also 425–300 μm or occasionally 300–250 μm) size fractions

following crushing, grinding, sieving and magnetic separation of whole rock samples. All separates were ultrasonically cleaned in a 10% HCl solution for ~15 minutes followed by thorough deionized water rinse and drying prior to oxygen isotope analysis. The purity of each separate was >99%. Olivine separates consisted of non-skeletal crystal fragments with <<1% spinel inclusions. Visibly sieved plagioclase and clinopyroxene crystals were avoided, although the final mineral separates sometimes exhibited slight variations in crystal color and clarity.

Oxygen isotope analyses were performed at the University of New Mexico stable isotope laboratory using the laser fluorination microanalytical technique of Sharp (1992). A Merchantek CO_2 laser catalyzed the reaction between approximately 2 mg of mineral and BrF_5 reagent. The oxygen gas liberated was purified and collected on a 13X molecular sieve prior to measurement of $\delta^{18}O_{mineral}$ values using a Finnigan MAT Delta XL mass spectrometer in dual-inlet mode.

The O isotope data were collected over 8 days on 3 separate trips to UNM during 2003–2004. Data are presented in Table 1. Sample measurements were typically duplicated and averaged, except where noted. All values are expressed in permil using standard delta notation relative to Standard Mean Ocean Water (SMOW). A garnet standard (UWG-2, where $\delta^{18}O$ = 5.8‰; Valley et al. 1995) was run prior to, during, and following each analytical session. In addition, an in-house quartz standard (Gee Whiz, where $\delta^{18}O$ = 12.5‰ relative to NBS-28 = 9.6‰) was periodically measured. The UWG-2 standard was run a total of 29 times during analyses and the mean value was 5.89‰ with 1σ = 0.07‰. Poor quality analyses (e.g. low yields) or unknown values obtained when the garnet standard exceeded 0.2‰ of the accepted value were excluded. Based on the duplicated unknowns and standard analyses, the 2σ uncertainty of the unknown analyses is considered ≤0.1‰ for ~65% of the samples.

Results

Table 1 summarizes $\delta^{18}O$ values for 29 olivine, 9 clinopyroxene, and 15 plagioclase separates. (Raw data and standard values can be viewed in the Supplemental Materials files). The higher standard deviations for $\delta^{18}O$ values in some mineral separates might reflect isotopic heterogeneities in the phenocrysts beyond analytical error. Previously published $\delta^{18}O_{whole\ rock}$ values have a one standard deviation = ±0.1‰ precision. Select geochemical data from Clynne (1993), Bacon et al. (1997), Borg et al. (1997), and Clynne (unpublished data) are included in the table.

Discussion

That the lavas in this study are primitive (with exceptions noted) has been previously demonstrated (e.g. Borg et al. 2002). The focus of this investigation is analysis of $\delta^{18}O$ values for constituent phases in selected lavas and then unraveling the sequences of open system processes that resulted in ^{18}O disequilibrium phase assemblage within the primitive lavas.

Oxygen isotope composition of olivine phenocrysts

Highly forsteritic olivine ($Fo_{86–91}$ from calc-alkaline lavas and $Fo_{86–88}$ from HAOT lavas) with spinel inclusions crystallized in chemical equilibrium with near-primary melts derived from the mantle (Clynne and Borg 1997). In Fig. 3a, $\delta^{18}O_{olivine}$ values are plotted against corresponding olivine phenocryst core Fo content. Lavas with crustal contamination (e.g. 035 and 031) are included in this plot to demonstrate how they compare with the other more primitive samples. Figure 3b illustrates $\delta^{18}O_{olivine}$ values plotted against corresponding $\delta^{18}O_{whole\ rock}$ values acquired by extraction with ClF_3 followed by isotope ratio mass spectrometry (Bacon et al. 1997; Borg et al. 1997). Samples deviate from closed-system fractionation for olivine in basaltic melts (Zhao and Zheng 2003).

Crustal contamination of magmas might move lava $\Delta^{18}O_{\text{whole rock-olivine}}$ (= $\delta^{18}O_{\text{whole rock}} - \delta^{18}O_{\text{olivine}}$) values significantly away from closed-system fractionation, but our samples are mostly primitive mafic melts. The relationship between $\Delta^{18}O_{\text{whole rock-olivine}}$ values and lava SiO_2 wt% is shown in Fig. 3c with the normal $\delta^{18}O$ array for closed system evolution of mantle derived melt by fractional crystallization (Bindeman et al. 2004). Non-laser-based methods for measuring $\delta^{18}O_{\text{whole rock}}$ values can be up to 0.4‰ too high (Eiler 2001) because small and variable amounts of rehydrated glass, low temperature alteration, and xenocrysts are included in the bulk analyses.

Glassy lavas are susceptible to low temperature hydration and alteration processes (Harmon and Hoefs 1995; Eiler 2001; Downes et al. 2001; Bindeman 2004; Hoefs 2004). Our glassiest samples lie above the closed-system crystal fractionation line. For example, sample 007 with the most hyalite of the sample suite and ~7% glass, has a $\delta^{18}O_{\text{whole rock}}$ value that is ~0.6‰ higher than nearby holocrystalline lavas. Lavas with low groundmass glass content have $\delta^{18}O_{\text{whole rock}}$ values that are probably minimally modified by rehydration. A model for producing melts with elevated $\delta^{18}O_{\text{whole rock}}$ values at all magma SiO_2 activities is required even with consideration of possible post-eruption modification.

$\delta^{18}O_{\text{olivine}}$ values: Hydrous fluid fluxing depleted peridotites under SMC region

Olivine phenocrysts in the forearc and arc axis calc-alkaline lavas have a slightly wider range of $\delta^{18}O_{\text{olivine}}$ values relative to the somewhat narrower range of $\delta^{18}O_{\text{olivine}}$ values for rear-arc calc-alkaline lavas, but no obvious cross-strike trend. HAOT lavas have olivine with the most restricted range of slightly elevated $\delta^{18}O_{\text{olivine}}$ values, despite their broad geographic distribution. For the SMC mafic calc-alkaline lavas, the parameter $(Sr/P)_N$ is an indicator of slab-derived fluid enrichment into peridotite melts, where N refers to normalization to compositions of primitive

mantle as defined by Sun and McDonough (1989). High and low $(Sr/P)_N$ value lavas generally occur in the forearc and rear-arc respectively, and $(Sr/P)_N$ correlates inversely with $^{87}Sr/^{86}Sr$ (Borg et al. 1997, 2002). Accordingly, the most highly fluid-fluxed depleted peridotite sources yield lavas with $(Sr/P)_N$ values > 5.5, whereas more fertile mantle with minor additions of slab-derived fluid produce lavas with $(Sr/P)_N$ values < 1.3. Further expansion of this relationship is illustrated in Fig. 4a ($\delta^{18}O_{olivine}$ values versus $(Sr/P)_N$) and Fig. 4b ($\delta^{18}O_{olivine}$ values versus $^{87}Sr/^{86}Sr$). The low $^{87}Sr/^{86}Sr$ slab-fluid component that fluxes depleted peridotites generate melts with high $\delta^{18}O$ olivine phenocrysts; the group of lavas with $^{87}Sr/^{86}Sr > 0.7035$ sourced from more fertile peridotite has similar phenocryst $\delta^{18}O_{olivine}$ values (Fig. 4b).

In Figs. 4b-d, $\delta^{18}O_{olivine}$ values are plotted versus whole rock $^{87}Sr/^{86}Sr$, $^{143}Nd/^{144}Nd$, and $^{176}Hf/^{177}Hf$. An ancient enrichment trajectory for a combination of subducted fluids and sediments added to MORB appears on each plot based upon modeling by Borg et al. (1997, 2002). For hydrous fluids from modern subduction of the northern segment of the Gorda plate, slab dewatering under the forearc region may have removed fluids more enriched than 20‰ from the oceanic crust. However, fluids derived from the hydrated slab peridotites below the gabbro layer probably includes a range of $\delta^{18}O$ values from ~15‰ fluids derived from deeper in the slab, and ~10‰ metamorphic fluids from chlorite dehydration reactions (Sheppard 1986). Hydrous slab fluid compositions from Borg et al. (1997, 2002) combined with $\delta^{18}O$ values of 15‰ are shown on all plots.

Discrete concentrated domains of oceanic sediment and upper altered basaltic oceanic crust (cf. Eiler et al. 2000) are likely variably faulted into the deeper levels of the slab (Chaytor et al. 2004). At least two geochemical results can be explained by this. First, a few of our samples may have been influenced by slab fluids derived from altered oceanic crust zone, an established

309 source of low $\delta^{18}O$ hydrous fluids (Gregory and Taylor 1981). Second, rising slab-derived fluids
310 generated from any source or melts encountering this type of mineralized domain may become
311 'spiked' (Borg et al. 1997). At lower pressures under the forearc and arc axis, 'spikes' from
312 channelized hydrous slab fluids (cf. Grove et al. 2002; Hildreth 2007) may be expressed most
313 clearly on the whole rock $^{87}Sr/^{86}Sr$ diagram (Fig. 4b) by the example mixing line(s) drawn
314 between the hydrous slab-derived fluid trajectory and a spike source. The continuum of $(Sr/P)_N$
315 values across the forearc and arc axis can be represented by a suite of similar mixing lines.
316 Analyses of melt inclusions in olivine phenocrysts from selected mafic tephra deposits in the
317 SMC area suggest dehydration reactions in chloritized mantle peridotites from the hot young
318 Gorda slab supplied some fluids (Walowski et al. 2015). In addition, the secondary melting of
319 materials near the slab surface postulated by Walowski et al. (2015) might be represented by
320 mixing lines similar to those in Fig. 4b. They report that primitive melts crystallizing olivine
321 were up to 3.4 wt.% H_2O in the Lassen area, but Figs. 4b-d are permissive of initial water
322 contents in SMC melts up to perhaps 6 wt.%.
323 Grove et al. (2002) estimate pre-eruptive melt H_2O content from <1 to >8 wt.% in primitive
324 magmas at Mt. Shasta. Stable isotope analysis of mafic phenocrysts in primitive lavas at Mt.
325 Shasta and Medicine Lake Volcano, with hydrous slab fluids and water-rich melts in the $\delta^{18}O$
326 value range of 8–14‰ (Martin et al. 2011), are comparable to our results. The edge of the
327 northern segment of the Gorda Plate subducts under Mt. Shasta, but the fractures on the northern
328 segment continue into its central deformation zone, which is subducted beneath the SMC region.
329 Detailed bathymetric maps of the Gorda Plate show active deformation including many
330 reactivated faults following original ridge fabric and complex networks of oblique shears to
331 accommodate regional plate motions (Chaytor et al. 2004). Heat flow from the slab window to

the south may induce additional strain in the slab that might further disrupt the $\delta^{18}O$ profiles that develop in undisturbed oceanic crust.

Coexisting olivine and clinopyroxene in SMC peridotite melts

Figure 5a illustrates $\delta^{18}O_{olivine}$ versus $\delta^{18}O_{cpx}$ values along with calculated equilibrium fractionations between clinopyroxene and olivine based on the olivine crystallization temperature range 1225–1275 °C of Clynne and Borg (1997), and using an average equilibrium fractionation line of $\Delta^{18}O_{diopside\text{-}forsterite}$ = 0.4‰ at ~1250 °C (Chiba et al. 1989). Compositional differences between mineral separates and endmember minerals (i.e. clinopyroxene versus diopside) on which calculated equilibrium fractionations are based, and uncertainty in crystallization temperatures are too small to account for the observed scatter in paired mineral $\delta^{18}O$ values (see Clynne (1993) for pyroxene analyses and Clynne and Borg (1997) for olivine analyses).

The data point distribution in Fig. 5a is indicative of open-system behavior (Gregory and Criss 1986) that affected the olivine phenocrysts and clinopyroxene phenocrysts in melts of changing ^{18}O content. To illustrate, consider a simple case where a melt lens near the top of the mantle contains ≤1% phenocrysts of olivine and clinopyroxene in ^{18}O equilibrium (point a). An amount of hydrous fluid roughly ~2% of the total melt contacts the magma. If instantaneous mixing produced a fully homogeneous liquid and adequate time for re-equilibration of olivine and clinopyroxene occurred, the new olivine-clinopyroxene equilibrium in the modified melt would be at point b. However, the self diffusion coefficient for ^{18}O in a 1 mm clinopyroxene phenocryst at 1250 °C is probably 10x slower than for ^{18}O in a 1 mm olivine phenocryst (cf. Bindeman 2008). Furthermore, the ^{18}O exchange reaction rate constants likely differ significantly for olivine and clinopyroxene (cf. Cole and Chackraborty 2001).

More complex processes involving multiple small fluid pulses introduced to the melts might occur, or melt extraction may coincide with slab-fluid interaction, leaving no time for isotopic equilibration. Occasionally two or more melt lenses may coalesce. Accordingly, it is unlikely that coexisting phases achieved ^{18}O equilibrium in such a dynamic magma environment where $\delta^{18}O_{melt}$ changes quickly relative to slower diffusion and kinetic rate limiting processes needed for resetting crystal phases.

Plagioclase crystallization and melt devolatilization during magma ascent

Anorthite content in plagioclase phenocrysts ranges from An_{60} to An_{90} in calc-alkaline lavas and from An_{72} to An_{83} in HAOT lavas (Clynne 1993). Clynne (1993) notes the correlation of phenocryst An content with whole rock geochemistry (in particular, Sr values) and speculates the calc-alkaline magmas were variably water-enriched. Figure 5b displays $\delta^{18}O_{whole\ rock}$ versus $\delta^{18}O_{plag}$ values for SMC mafic magmas.

The calc-alkaline magmas are likely to be unusually buoyant from fluid-enrichment in the mantle. If plagioclase crystallization began under elevated x_{H_2O} conditions (cf. Hammer 2008), those phenocrysts should record melt ^{18}O enrichment. However, plagioclase crystallization during magma ascent (Clynne and Borg 1997; Borg et al. 1997) would have occurred simultaneously with melt devolatilization. The ~1150 $^{\circ}C$ isotherm for anorthite in a basaltic melt (Zhao and Zheng 2003) is a reasonable crystallization temperature, but accounting for shifts in ^{18}O fractionation in plagioclase due to an increasing albite component is not feasible with this study. At eruption, water lost from the melt could have reduced $\delta^{18}O_{melt}$ by 0.4‰ or more (Eiler 2001) as evidenced by some samples in Figs. 3b and 3c. Melt ^{18}O enrichment may be higher yet in samples where devolatilization of CO_2, SO_2 or both occurred (Walowski et al. 2016).

Quaternary climate fluctuations and evidence for temporary ponds and lakes are common in this region, and orographic effects generate local and extreme variability in annual precipitation. In the Hat Creek Basin, the range of $\delta^{18}O$ values for cold springs is −14.0 to −9.1‰, and for lakes is −8.7 to −4.2‰ (Rose et al. 1996). Meteoric water infiltration especially into more vesicular lavas may produce cryptic low temperature alteration that can reduce $\delta^{18}O_{whole\ rock}$ relative to $\delta^{18}O_{plag}$ values (Fig. 5b). The effect of meteoric water infiltration into the vesicular HAOT lava (013) is likely the cause of the ^{18}O shift after plagioclase crystallization in the hotter, drier tholeiitic magma.

Finally, the ^{18}O disequilibria of the solids and melt suggest that all open system processes acting on magma were often swift enough to significantly change at least one phase and induce varying levels of $\delta^{18}O$ heterogeneity of other phases. For example, the poor correlation of $\delta^{18}O_{olivine}$ with $(Sr/P)_N$ in (Fig. 4a) could indicate that elevated ^{18}O slab-derived hydrous fluid interacted with discrete mantle melt lenses, but it reveals nothing about the degree of ^{18}O isotopic equilibrium achieved between the melt and crystal phases or isotopic homogeneity of the magma. Perhaps only limited ^{18}O equilibration would be possible in the upper mantle melt lenses because buoyancy would drive melt extraction.

Comparison with Cascade arc primitive lavas to the north

To compare the SMC with other Cascade arc at primitive lavas (Fig. 6), we begin with the Mt. Adams volcanic field (MAVF), where Jicha et al. (2009) concluded that only a minor contribution of fluid derived from subducted sediment is present in the mantle source. Phenocryst $\delta^{18}O_{olivine}$ values in MAVF primitive lavas reflect minor ^{18}O enrichment in the source, while $\delta^{18}O_{olivine}$ values from dryer HAOT magmas may have originated from a more depleted peridotite. Continuing south into the central Oregon Cascades, Ruscitto et al. (2010)

400 analyzed fluid inclusions in olivine phenocrysts, as well as $\delta^{18}O_{olivine}$ values for host olivine from
401 non-primitive mafic calc-alkaline lavas for which numerical restoration was performed to reach
402 initial melt compositions. The investigators concluded a seawater-like slab fluid fluxed depleted
403 peridotite in the mantle wedge, sometimes with a Sr-rich component added, and initial melts
404 ranged from 1.7–3.6 wt.% H_2O.

405 Mt. Shasta overlies the projection of the subducting transform fault (Blanco Fracture Zone)
406 between the main Juan de Fuca Plate and the northern segment of the Gorda Plate (Fig. 1a).
407 Primitive mafic andesites at Mt. Shasta have pre-eruptive water contents of 6.5 wt.% and Grove
408 et al. (2005) further argued for 10–15 wt.% H_2O in some magmas where initial mantle melts
409 were "water oversaturated". Martin et al. (2011) confirm the slab-derived fluid input for Mt.
410 Shasta primitive mafic lavas. The range of $\delta^{18}O_{olivine}$ values is strikingly similar to those from
411 SMC calc-alkaline lavas. Although many of the SMC primitive melts may have had ~3.4 wt.%
412 H_2O during olivine crystallization (Walowski et al. 2015), our work supports higher, transient
413 releases of hydrous slab-derived fluids from the deformed Gorda Plate during subduction. The
414 modern addition of hydrous fluids may include up to 6 wt.% of deep slab-derived hydrous fluid
415 ranging from 15‰ in the forearc to 10‰ metamorphic reaction fluids farther east with sporadic
416 release of slab-fluids from altered-upper oceanic basaltic crust (0–6‰), which might yield low
417 $\delta^{18}O_{whole\ rock}$ values (cf. Walowski et al. 2016). In addition, although generally depleted in LILE,
418 the SMC lithospheric mantle has been metasomatized in some components (e.g. Fe, Al, and
419 exhibits a weak subduction signature), probably as a result of passage of arc magmas
420 intermittently at least since the early Cretaceous.

421 The modern SMC mantle lithosphere, a heterogeneous collage of mantle domains enriched
422 during ancient subduction (Leeman et al. 1990; Clynne 1993; Clynne and Borg 1997; Borg et al.

1997; 2000; 2002), is the source of HAOT magmas (Borg et al. 1997, 2002). Our HAOT $\delta^{18}O_{olivine}$ values are consistent with ^{18}O enrichment by ancient sediment incorporation into the mantle, supplemented by modern enrichment via diffuse regional metasomatism (e.g. up to 2 wt.% by hydrous slab-fluids in Figs. 4b-d). Consider that HAOT primitive melts at rear-arc Medicine Lake Volcano (constructed on a similar terrane collage) may be least influenced by modern fluids and sediment input because Mt. Shasta provides pressure relief for excess slab volatiles (Donnelly-Nolan et al. 2008). Martin et al. (2011) believe the source of HAOT melts at Mt. Shasta is ^{18}O enriched through focused metasomatic processes. Accordingly, the SMC mantle lithosphere may be affected by regionally distributed volatiles that pass through it leading to HAOT melts that are relatively ^{18}O enriched over HAOTs at Medicine Lake Volcano, but less than those at Mt. Shasta. Perhaps additional support for this argument are the estimates of initial magmatic volatiles (CO_2 and SO_2) from melt inclusions in olivine (Walowski et al. 2016) and volcanic CO_2 component present in cold springs in the Hat Creek drainage (Rose et al. 1996).

Implications

Clearly, more detailed $\delta^{18}O$ investigations are needed to determine timing of slab-fluid entry into these melts. Our analysis of mineral separates suggests it may be possible to gain more insight into melt or fluid additions to the deep reservoirs from examining individual olivine phenocrysts. Ion microprobe analyses for $\delta^{18}O$ profiling across selected single phenocrysts is needed for detailed chemical and isotopic information to clarify phase relationships and zoning or diffusion profiles from which process rates and timing constraints for fluid (or melt) addition or loss may be determined. In particular, 020 has olivine and clinopyroxene with chemically similar Cr-spinel inclusions (Clynne 1993) and it may be especially valuable for understanding some

conditions in the mantle peridotite where segregated melt coalesces. In situ isotopic analysis of clinopyroxene by laser ablation for $^{87}Sr/^{86}Sr$ and $^{143}Nd/^{144}Nd$ might yield details regarding the sequence of events in the upper mantle melt lens. For lavas postulated to be blends of primitive CAB and HAOT melts (e.g. 032), are multiple populations olivine phenocrysts with distinct $\delta^{18}O_{olivine}$ values or profiles detectable? Lastly, larger skeletal olivines might provide $\delta^{18}O_{skeletal\ olivine}$ values to supplement plagioclase analyses for open system processes during final shallow magma ascent and melt degassing.

Acknowledgments

We thank Grace Winer for preparing mineral separates, Viorel Atudorei and Dan Breeker for their assistance in the stable isotope laboratory of the Earth and Planetary Sciences Department at the University of New Mexico, and P. B. Larson, A. Matthews, J. R. Bowman, and P. I. Nabelek for stimulating discussions of the mineral $\delta^{18}O$ data. M. Skidmore provided valuable input in the earlier stages of this project. This manuscript significantly benefited from improvements based on thoughtful reviews by C. Bacon, L. Hammersley, W. Leeman, O. Müntener, M. Loewen, and two anonymous reviewers. Funding for this work was provided by the National Science Foundation (EAR 9983769) to T. Feeley and a Geological Society of America grant (7821-04) to Underwood for field work. Any use of trade, firm, or product names is for descriptive purposes only and does not imply endorsement by the U.S. Government.

References

Bacon, C.R., Bruggman, P.E., Christiansen, R.L., Clynne, M.A., Donnelly-Nolan, J.M., and Hildreth, W. (1997) Primitive magmas at five Cascade volcanic fields: Melts from hot, heterogeneous sub-arc mantle. Canadian Mineralogist, 35, 397–423.Bartels, K.S., Kinzler, R.J., and Grove, T.L. (1991) High pressure phase relations of primitive high-alumina basalts from Medicine Lake volcano, northern California. Contributions to Mineralogy and Petrology, 108, 253–270.

Bindeman, I. (2008) Oxygen isotopes in mantle and crustal magmas as revealed by single crystal analysis. In K. Putirka, and F. Tepley, Eds., Minerals, Inclusions and Volcanic Processes, 69, p. 445–478. Reviews in Mineralogy and Geochemistry, Mineralogical Society of America, Washington, D.C.

Bindeman, I.N, Ponomareva, V.V., Bailey, J.C., and Valley, J.W. (2004) Volcanic arc of Kamchatka: A province with high-$\delta^{18}O$ magma sources and large-scale $^{18}O/^{16}O$ depletion of the upper crust. Geochimica et Cosmochimica Acta, 68, 841–865.

Blakely, R.J., Christiansen, R.L., Guffanti, M., Wells, R.E., Donnelly-Nolan, J.M., Muffler, L.J.P., Clynne, M.A., and Smith, J.G. (1997) Gravity anomalies, Quaternary vents, and Quaternary faults in the southern Cascade Range, Oregon and California: Implications for arc and backarc evolution. Journal of Geophysical Research, 102, 22513–22527.

Borg, L.E., Blichert-Toft, J., and Clynne, M.A. (2002) Ancient and modern subduction zone contributions to the mantle sources of lavas from the Lassen region of California inferred from Lu-Hf isotopic systematics. Journal of Petrology, 43, 705–723.

Borg, L.E., Brandon, A.D., Clynne, M.A., and Walker, R.J. (2000) Re-Os isotopic systematics of primitive lavas from the Lassen region of the Cascade arc, California. Earth and Planetary Science Letters, 177, 301–317.

Borg, L.E., Clynne, M.A., and Bullen, T.D. (1997) The variable role of slab-derived fluids in the generation of a suite of primitive calc-alkaline lavas from the southernmost Cascades, California. Canadian Mineralogist, 35, 425–452.

Borg, L.E. (1995) The origin and evolution of magmas from the Lassen region of the southernmost Cascades, 229 p. Dissertation, University of Texas, Austin.

Bullen, T.D., and Clynne, M.A. (1990) Trace element and isotopic constraints on magmatic evolution at Lassen Volcanic Center. Journal of Geophysical Research, 95, 19671–19691.

Bullen, T.D., and Clynne, M.A. (1989) Coupled spatial, chemical, and isotopic characteristics of primitive lavas from the Lassen region, California. IAVCEI Continental Magmatism Abstracts. New Mexico Bureau of Mines and Mineral Resources, Bulletin 131, p. 33.

Chauvel, C., and Blichert-Toft, J. (2001) A hafnium isotope and trace element perspective on melting of the depleted mantle. Earth and Planetary Science Letters, 190, 137–151.

Chaytor, J.D., Goldfinger, C., Dziak, R.P., and Fox, C.G. (2004) Active deformation of the Gorda plate: Constraining deformation models with new geophysical data. Geology, 32, 353–356.

Chiba, H., Chacko, T., Clayton, R.N., and Goldsmith, J.R. (1989) Oxygen isotope fractionations involving diopside, forsterite, magnetite, and calcite; Application to geothermometry. Geochimica et Cosmochimica Acta, 53, 2985–2995.

Clynne, M.A., and Borg, L.E. (1997) Olivine and chromian spinel in primitive calc-alkaline and tholeiitic lavas from the southernmost Cascade range, California: A reflection of relative fertility of the source. Canadian Mineralogist, 35, 453–472.

Clynne, M.A. (1993) Geologic studies of the Lassen Volcanic Center, Cascade Range, California, 413 p. Dissertation, University of California, Santa Cruz.

Cole, D.R., and Chackraborty, S. (2001) Rates and mechanisms of isotopic exchange. In J.W. Valley, and D.R. Cole, Eds., Stable Isotope Geochemistry, 43, p. 83–223. Reviews in Mineralogy and Geochemistry, Mineralogical Society of America, Washington, D.C.

Davis, A.S., Clague, D.A., Cousens, B.L., Keaten, R., and Paduan, J.B. (2008) Geochemistry of basalt from the North Gorda segment of the Gorda Ridge: Evolution toward ultraslow spreading ridge lavas due to decreasing magma supply. Geochemistry Geophysics Geosystems, 9, Q04004, doi:10.1029/2007GC001775.

Day, H.W., and Bickford, M.E. (2004) Tectonic setting of the Jurassic Smartville and Slate Creek complexes, northern Sierra Nevada, California. Geological Society of America Bulletin, 116, 1515–1528.

Dickinson, W.R. (2008) Accretionary Mesozoic-Cenozoic expansion of the Cordilleran continental margin in California and adjacent Oregon. Geosphere, 4, 329–353.

Donnelly-Nolan, J.M., Grove, T.L., Lanphere, M.A., Champion, D.E., and Ramsey, D.W. (2008) Eruptive history and tectonic setting of Medicine Lake Volcano, a large rear-arc volcano in the southern Cascades. Journal of Volcanology and Geothermal Research, 177, 313–328.

Downes, H., Thirlwall, M.F., and Trayhorn, S.C. (2001) Miocene subduction-related magmatism in southern Sardinia: Sr-Nd- and oxygen isotopic evidence for mantle source enrichment. Journal of Volcanology and Geothermal Research, 106, 1–21.

Dziak, R.P., Fox, C.G., Bobbitt, A.M., and Goldfinger, C. (2001) Bathymetric map of the Gorda Plate: Structural and geomorphological processes inferred from multibeam surveys. Marine Geophysical Research, 22, 235–250.

Eiler, J.M. (2001) Oxygen isotope variations of basaltic lavas and upper mantle rocks. In J.W. Valley, and D.R. Cole, Eds., Stable Isotope Geochemistry, 43, p. 319–364. Reviews in Mineralogy and Geochemistry, Mineralogical Society of America, Washington, D.C.

Eiler, J.M., Crawford, A., Elliott, T., Farley, K.A., Valley, J.W., and Stolper, E.M. (2000) Oxygen isotope geochemistry of oceanic-arc lavas. Journal of Petrology, 41, 229–256.

Gregory, R.T., and Criss, R.E. (1986) Isotopic exchange in open and closed systems. In: J.W. Valley, H.P. Taylor, and J.R. O'Neil, Eds., Stable Isotopes in High Temperature Geological Processes, 16, p. 91–127. Reviews in Mineralogy, Mineralogical Society of America, Washington, D.C.

Gregory, R.T., and Taylor, H.P. (1981) An oxygen isotope profile in a section of Cretaceous oceanic crust, Samail ophiolite, Oman: Evidence for $\delta^{18}O$ buffering of the oceans by deep (>5 km) seawater-hydrothermal circulation at mid-ocean ridges. Journal of Geophysical Research, 86, 2737–2755.

Grove, T.L., Baker, M.B., Price, R.C., Parman, S.W., Elkins-Tanton, L.T., Chatterjee, N., and Müntener, O. (2005) Magnesian andesite and dacite lavas from Mt. Shasta, northern California: products of fractional crystallization of H_2O-rich mantle melts. Contributions to Mineralogy and Petrology, 148, 542–565.

Grove, T.L., Parman, S.W., Bowring, S.A., Price, R.C., and Baker, M.B. (2002) The role of an H_2O-rich fluid component in the generation of primitive basaltic andesites and andesites from the Mt. Shasta region, N. California. Contributions to Mineralogy and Petrology, 142, 375–396.

Guffanti, M., Clynne, M.A., Smith, J.G., Muffler, L.P.J., and Bullen, T.D. (1990) Late Cenozoic volcanism, subduction, and extension in the Lassen region of California, southern Cascade range. Journal of Geophysical Research, 95, 19453–19464.

Guffanti, M., Clynne, M.A., and Muffler, L.J.P. (1996) Thermal and mass implications of magmatic evolution in the Lassen volcanic region, California, and minimum constraints on basalt influx to the lower crust. Journal of Geophysical Research, 101, 3003–3013.

Gulick, S.P.S., Meltzer, A.S., Henstock, T.J., Levander, A. (2001) Internal deformation of the southern Gorda plate: Fragmentation of a weak plate near the Mendocino triple junction. Geology, 29, 691–694.

Harmon, R.S., and Hoefs, J. (1995) Oxygen isotope heterogeneity of the mantle deduced from global ^{18}O systematics of basalts from different geotectonic settings. Contributions to Mineralogy and Petrology, 120, 95–114.

Hammer, J.E. (2008) Experimental studies of the kinetics and energetic of magma crystallization. In K. Putirka, and F. Tepley, Eds., Minerals, Inclusions and Volcanic Processes, 69, p. 9–59. Reviews in Mineralogy and Geochemistry, Mineralogical Society of America, Washington, D.C.

Hildreth, W. (2007) Quaternary Magmatism in the Cascades—Geologic Perspectives. United States Geological Survey Professional Paper 1744, 125 p.

Hoefs, J. (2004) Stable isotope geochemistry, 244 p. Springer-Verlag, New York.

Jicha, B.R., Hart, G.L., Johnson, C.M., Hildreth, W., Beard, B.L., Shirey, S.B., and Valley, J.W. (2009) Isotopic and trace element constraints on the petrogenesis of lavas from the Mount Adams volcanic field, Washington. Contributions to Mineralogy and Petrology, 157, 189–207.

Leeman, W.P., Smith, D.R., Hildreth, W., Palacz, Z., and Rogers, N. (1990) Compositional diversity of Late Cenozoic basalts in a transect across the Southern Washington Cascades: Implications for subduction zone magmatism. Journal of Geophysical Research, 95, 19561–19582.

Martin, E., Bindeman, I., and Grove, T.L. (2011) The origin of high-Mg magmas in Mt Shasta and Medicine Lake volcanoes, Cascade Arc (California): higher and lower than mantle oxygen isotope signatures attributed to current and past subduction. Contributions to Mineralogy and Petrology, 162, 945–960.

Mattey, D., Lowry, D., and Macpherson, C. (1994) Oxygen isotope composition of mantle peridotite. Earth and Planetary Science Letters, 128, 231–241.

McBirney, A.R. (1968) Petrochemistry of the Cascade andesite volcanoes. Oregon Department of Geology and Mineral Industries, Bulletin 62, 101–107.Miller, M.M., Johnson, D.J., Rubin, C.M., Dragert, H., Wang, K., Qamar, A., and Goldfinger, C. (2001) GPS-determination of along-strike variation in Cascadia margin kinematics: Implications for relative plate motion, subduction zone coupling, and permanent deformation. Tectonics, 20, 161–176.

Rose, T.P., Davisson, M.L., and Criss, R.E. (1996) Isotope hydrology of voluminous cold springs in fractured rock from an active volcanic region, northeastern California. Journal of Hydrology, 179, 207–236.

Ruscitto, D.M., Wallace, P.J., Johnson, E.R., Kent, A.J.R., and Bindeman, I.N. (2010) Volatile contents of mafic magmas from cinder cones in the Central Oregon High Cascades: Implications for magma formation and mantle conditions in a hot arc. Earth and Planetary Science Letters, 298, 153–161.Sharp, Z.D. (1992) *In situ* laser microprobe techniques for stable isotope analysis. Chemical Geology, 101, 3–19.

Sheppard, S.M.F. (1986) Characterization and isotopic variations in natural waters. In: J.W. Valley, H.P. Taylor, and J.R. O'Neil, Eds., Stable Isotopes in High Temperature Geological Processes, 16, p. 165–183. Reviews in Mineralogy, Mineralogical Society of America, Washington, D.C.

Sun, S.-S., and McDonough, W.F. (1989) Chemical and isotopic systematics of oceanic basalts: Implications for mantle composition and processes. In: A.D. Saunders, and M.J. Norry, Eds., Magmatism in the Ocean Basins, Geological Society, London, Special Publications, 42, p. 313–345.

Trehu, A., and The Mendocino Working Group (1995) Pulling the rug out from under California: Seismic images of the Mendocino Triple Junction region. EOS Transactions of the American Geophysical Union, 76, 380–381.

Valley, J.W., Kitchen, N., Kohn, M.J., Niendorf, C.R., and Spicuzza, M.J. (1995) UWG-2, a garnet standard for oxygen isotope ratios: Strategies for high precision and accuracy with laser heating. Geochimica et Cosmochimica Acta 59, 5226–5231.

Walowski, K.J., Wallace, P.J., Clynne, M.A., Rasmussen, D.J. and Weis, D. (2016) Slab melting and magma formation beneath the southern Cascade arc. Earth and Planetary Science Letters, http//dx.doi.org/10.1016/j.epsl.2016.03.044.

Walowski, K.J., Wallace, P.J., Hauri, E.H., Wada, I., and Clynne, M.A. (2015) Slab melting beneath the Cascade Arc driven by dehydration of altered oceanic peridotite. Nature Geoscience, 8, 404–409.

Zhao, Z.-F., and Zheng, Y.-F. (2003) Calculation of oxygen isotope fractionation in magmatic rocks. Chemical Geology, 193, 59–80.

This is a preprint, the final version is subject to change, of the American Mineralogist (MSA)
Cite as Authors (Year) Title. American Mineralogist, in press.
(DOI will not work until issue is live.) DOI: http://dx.doi.org/10.2138/am-2016-5588CCBY

Appendix

Petrography

Although the lavas studied are generally sparsely phyric, each sample contains at least one olivine phenocryst population that always includes euhedral or slightly rounded crystals up to ~3 mm across. The large olivine phenocrysts host chromian spinel inclusions (Fig. 2a) that were investigated by Clynne and Borg (1997). Some lavas contain smaller skeletal olivine phenocrysts (Fig. 2d) and in these rocks, the larger olivine phenocrysts commonly have thin, sometimes more Fe-rich, hopper growths. All rear-arc and approximately half of the forearc lavas contain skeletal olivine microphenocrysts. In the study area, at least half of the calc-alkaline forearc lavas (1009, 017, 015, 020, 036, 033, 037, 034 and 032) and northern arc axis lavas (012 and 001) have a sub-population (<3%) of large olivine phenocrysts with orthopyroxene coronas. Some lavas contain olivine-bearing crystal clots (012, 013, 031, 032, 033, 035, 036 and 039).

Orthopyroxene crystals >0.25 mm across are present in three calc-alkaline basaltic andesitic lavas (036 and 037 in the southern forearc, and 001 on the northern arc axis) and one northwest forearc calc-alkaline basaltic lava (017). The orthopyroxene crystals often include minor populations with nonequilibrium textures including resorption and sieved zones with clear rim overgrowth, and sutured grain boundaries in crystal clots.

Clinopyroxene crystals (Figs 2b) are restricted to calc-alkaline lavas where they occur in glomerocrysts (sometimes with olivine) and as individual phenocrysts. Clinopyroxene is most common in lavas from the northwestern forearc and arc axis regions. It is sporadically present in lavas from the southwest forearc and sparse in lavas erupted from back-arc vents. In several lavas, particularly those from the northwestern forearc region, clinopyroxene crystals have sieved zones surrounded by clear overgrowths. Clinopyroxene in glomerocrysts frequently have

655 sutured grain boundaries, in addition to resorption/regrowth textures such as sieved horizons
656 surrounding clear cores. Cumulate olivine and pyroxene is present in 036 (cf. Clynne 1993).
657 In 6 of 11 lavas collected from the southern forearc and arc axis areas, no plagioclase
658 phenocrysts are present; the other samples contain multiple plagioclase populations including
659 both zoned (Fig. 2c) and sieved crystals with clear overgrowths. In the northwest forearc and
660 northern arc axis areas, multiple plagioclase populations are often present; only two samples
661 (014 and HAOT 013) have a single population of clear plagioclase. Five of nine northeast rear-
662 arc lavas contain multiple plagioclase populations. Finally, multiple plagioclase populations
663 including sieved crystals with clear overgrowths are present in HAOT samples 002 and 030.
664 Groundmass textures of the calc-alkaline lavas range from intergranular to hyalo-ophitic,
665 and the three HAOT lavas are sub-ophitic to intersertal (cf. Clynne 1993). Proportions and
666 overall coarseness of groundmass phases (i.e. plagioclase, pyroxenes, opaques, and olivine) vary
667 among the lavas; 22 samples contain <1% glass, while the three glassiest hyalo-ophitic samples
668 contain 7–10% glass. Diktytaxitic textures are common in HAOT samples. Vesicularity is low
669 (<1%) in ~50% of the lavas; other samples have heterogeneous vesicles sizes and shapes with up
670 to 20% vesicularity in a few cases.
671 Many samples (69%) contain olivine with thin iddingsite coatings. Other secondary mineral
672 phases present include hyalite (31% of the samples), hydrous iron oxides (31% of the samples),
673 and zeolites (17% of the samples). In nearly all samples, the secondary minerals constitute <<1
674 vol% of the rock. Although about 40% of the lavas contain quartz xenocrysts or small hornfels
675 xenoliths, these materials constitute << 1 vol% of the rock in all cases.
676

Figure Captions

Figure 1. (a) Map of the Cascade volcanic arc tectonic setting modified after McBirney (1968). Accreted oceanic lithosphere of the Columbia Embayment is bounded by dashed lines. Late Cenozoic volcanic rocks from High Cascades are dark gray fill with major composite volcanoes and volcanic centers indicated by triangles: LVC = Lassen Volcanic Center, MS = Mount Shasta, MLV = Medicine Lake Volcano, MMc = Mount McLoughlin, CLV = Crater Lake Volcano, NV = Newberry Volcano, TS = Three Sisters, MJ = Mount Jefferson, MH = Mount Hood, MSH = Mount Saint Helens, MA = Mount Adams, SVF = Simcoe Volcanic Field, MR = Mount Rainier, GP = Glacier Peak, MB = Mount Baker, MG = Mount Garibaldi, MC = Mount Cayley, MM = Meager Mountain. SMC = Southernmost Cascades (inset box). **(b)** Map of sample sites for SMC little-evolved mafic lavas in this study. Calc-alkaline lavas erupted from vents located between the trench and modern arc axis (i.e. projection of upper slab surface depth of ~100 km to over-riding plate surface) are in the forearc (circles). Rear-arc vents (triangles) are east of the arc axis (squares). CA samples symbols with $(Sr/P)_N > 3.2$ are solid filled and calc-alkaline samples with $(Sr/P)_N < 3.2$ are open (Borg et al. 1997). HAOT lavas = diamonds.

Figure 2. (a) Olivine phenocryst with spinel inclusions from LF02-034 in ppl. **(b)** Clinopyroxene phenocryst from LF02-012 in xp. **(c)** Plagioclase phenocryst with zoning and microphenocrysts from LF02-001 in xp. **(d)** Skeletal olivine from LF02-031 in xp. Scale bar in all images is 0.2 mm.

Figure 3. (a) Olivine $\delta^{18}O$ values versus olivine phenocryst core Fo content (Clynne 1993; Borg 1995; Clynne and Borg 1997). **(b)** Olivine $\delta^{18}O$ values by laser fluorination versus whole rock $\delta^{18}O$ values by resistance heating of SMC little-evolved mafic lavas (Clynne 1993; Borg et al. 1997; Bacon et al. 1997). An equilibrium line for $\delta^{18}O_{melt} = \delta^{18}O_{olivine} + \Delta^{18}O_{glass\text{-}olivine}$ drawn for closed system crystal fractionation, where $\Delta^{18}O_{glass\text{-}olivine} = 0.7‰$ for olivine (heavy line) basaltic melt (Zhao and Zheng 2003). **(c)** Measured difference values ($\Delta^{18}O_{whole\ rock\text{-}olivine} = \delta^{18}O_{whole\ rock} - \delta^{18}O_{olivine}$) versus whole rock SiO_2 content. Samples with 5–10 vol.% groundmass glass have large symbols with italicized labels. Crustally contaminated LF02-035 and LF02-031, and cumulate-bearing LF02-036 are labeled in boldface. The thick line represents the expected range of melts produced by closed-system crystal fractionation as described in (b), but using the normal $\delta^{18}O$ array from Bindeman et al. (2004). Symbols as described in Fig. 1b.

Figure 4. (a) $\delta^{18}O_{olivine}$ values versus whole rock $(Sr/P)_N$. **(b)** Phenocryst $\delta^{18}O_{olivine}$ values versus whole rock $^{87}Sr/^{86}Sr$. **(c)** Phenocryst $\delta^{18}O_{olivine}$ values versus whole rock $^{143}Nd/^{144}Nd$. **(d)** Phenocryst $\delta^{18}O_{olivine}$ values versus whole rock $^{176}Hf/^{177}Hf$. Silicate melts are solid lines with tick marks in 1 wt.% increments and hydrous fluids are dashed lines with tick marks in 1 wt.% increments. Mixing lines between hydrated peridotite and spike have tick marks at 0.1 wt.% increments. North Gorda glass MORB from Davis et al. (2008); East Pacific MORB from Chauvel and Blichert-Toft (2001). Symbols as described in Fig. 1b. (All model concentrations are tabulated in Supplemental Materials Model Values file).

720

721 **Figure 5. (a)** Olivine and clinopyroxene δ-δ plot for phenocryst separates. Calculated
722 $\Delta^{18}O_{diopside\text{-}forsterite}$ is 0.41‰ at 1225 °C and 0.38‰ at 1275 °C from Chiba et al. (1989). Dotted
723 lines are example trajectories that connect points a and b described in the text. Non-primitive
724 sample 017 has core olivine $Fo_{82.5}$ and $(Sr/P)_N < 0.32$. **(b)** Plagioclase and whole rock δ-δ plot.
725 Fractionation factors for ^{18}O between anorthite and basalt were calculated at 1150 °C using the
726 relationships of Zhao and Zheng (2003). The effects of melt devolatilization during magma
727 ascent and meteoric water infiltration in lava flows on $\delta^{18}O_{whole\ rock}$ values are depicted with
728 arrows. Symbols as in Fig. 1b.

729

730 **Figure 6.** Oxygen isotope compositions for olivine phenocrysts from SMC mafic lavas and
731 selected primitive Cascade mafic lavas. Symbols for SMC samples are described in Fig. 1b.
732 Olivine oxygen isotope values from calc-alkaline lavas from Mt. Shasta, Medicine Lake
733 Volcano, Central Oregon Cascades and the Mt. Adams Volcanic Field are indicated by 'X' and
734 olivine in HAOT lavas are smaller '+' symbols (Martin et al. 2011; Ruscitto et al. 2010; Jicha et
735 al. 2009). Mantle peridotite $\delta^{18}O_{olivine}$ range is indicated by the variably shaded area (Mattey et
736 al. 1994).

737

738

This is a preprint, the final version is subject to change, of the American Mineralogist (MSA)
Cite as Authors (Year) Title. American Mineralogist, in press.
(DOI will not work until issue is live.) DOI: http://dx.doi.org/10.2138/am-2016-5588CCBY

Table 1. Summary of mineral and whole rock $^{18}O/^{16}O$ data for selected Southernmost Cascades mafic lavas.

Sample number	Equivalent sample number [a]	Type / Locale [c]	SiO_2 wt % [a]	MgO wt % [a]	Mg# [a]	$(Sr/P)_N$ [a]	$\delta^{18}O_{WR}$ ‰ [a]	olivine $\delta^{18}O$ ‰ [b]		cpx $\delta^{18}O$ ‰ [b]		plag $\delta^{18}O$ ‰ [b]	
								Mean	1 Std Dev	Mean	1 Std Dev	Mean	1 Std Dev
LC86-1009		CA / FA	58.17	7.57	70.6	6.59	6.9	5.59					
LF02-037	LC88-1303	CA / FA	57.61	7.49	70.8	4.79	7.0	5.88	0.13	6.00	0.04	10.89	
LF02-033	LC88-1310	CA / FA	56.14	10.20	77.3	5.88	7.4	5.90	0.01				
LF02-036[d]	LC88-1301	CA / FA	55.69	14.35	82.3	4.73	6.8	5.80	0.05	6.06			
LF02-019	LC86-1006	CA / FA	54.49	8.34	72.7	2.42	6.7	5.62	0.01			9.06	
LF02-035[e]	LC88-1305	CA / FA	53.75	10.87	76.7	3.28	7.8	6.31	0.03				
LF02-015[d]	LB92-168; LC92-1703	CA / FA	53.45	7.65	69.5	4.90	6.6	5.84	0.00	5.91	0.08		
LF02-014[d]	LB92-167; LC92-1702	CA / FA	53.09	8.15	71.4	5.81	6.2	5.31	0.08	5.58	0.07	6.11	0.08
LC88-1308		CA / FA	51.46	9.09	73.3	5.96	7.2	5.62	0.05				
LF02-020[e]	LC86-1005	CA / FA	51.30	11.10	71.5	3.76	5.6	5.63	0.10	5.58		6.32	
LF02-017[d]	LB92-166; LC92-1701	CA / FA	51.09	11.06	75.7	2.89	6.6	5.61	0.03	5.46	0.03	7.09	
LF02-031	LC88-1314	CA / FA	50.82	8.43	68.1	1.47	7.2	6.24	0.10				
LF02-032[e]	LC88-1312	CA / FA	50.80	9.97	70.1	5.36	6.9	5.87	0.11			6.71	0.09
LF02-034[e]	LC87-1056	CA / FA	50.57	8.24	70.5	5.10	6.4	5.96	0.10				
LF02-012	LC85-743	CA / AA	58.76	5.90	69.3	5.72	6.9	5.74	0.05	5.75	0.09	10.49	
LF02-001	LC83-255	CA / AA	54.49	7.73	73.2	5.47	6.9	5.49	0.05	5.70		7.98	
LF02-039	LC88-1371	CA / AA	51.99	8.34	69.2	3.21	5.7	5.85	0.04	6.22		6.48	
LF02-038	LM92-2443	CA / AA	51.20	8.15	68.5	1.55	6.5	6.01	0.07				
LF02-006	LC86-831	CA / RA	52.81	7.09	66.7	1.52	6.7	5.89	0.01			9.32	
LF02-005	LC86-829	CA / RA	51.50	9.20	73.7	3.89	6.7	5.67	0.04			6.34	
LF02-007	LC85-671	CA / RA	51.35	8.05	68.0	1.67	7.4	5.63	0.03				
LF02-004	LM91-2116	CA / RA	51.17	10.15	75.5	3.32	6.0	5.59	0.05			6.01	0.14
LF02-011	LM87-1333	CA / RA	50.80	7.75	68.1	1.52	6.7	5.49	0.05			7.28	
LF02-009	LC82-905	CA / RA	50.37	8.43	69.0	1.68	5.9	5.65	0.20				
LF02-010	LM87-1384	CA / RA	49.64	10.67	74.2	1.35	6.9	5.87	0.04			8.77	
LF02-008	LC86-834	CA / RA	49.37	10.46	72.6	1.92	6.4	5.79	0.05				
LF02-030	LC86-1046	HAOT / AA	48.20	10.10	66.5		6.1	5.66	0.01				
LF02-013	LC84-514	HAOT / AA	48.58	9.90	69.2		5.8	5.74	0.05			6.35	0.02
LF02-002	LC84-569	HAOT / RA	49.58	8.71	67.8		5.8	5.54	0.01				

[a] Data from cross-referenced samples of Borg et al. (1997), Bacon et al. (1997), Clynne (1993), Clynne unpublished data. Mg# = 100 [Mg] / ([Mg] + [Fe^{2+}]).

[b] All oxygen values are reported in ‰ SMOW and are uncorrected. Single values have no standard deviation.

[c] Lava type: CA = calc-alkaline and HAOT = high alumina olivine tholeiite. Location relative to arc axis: FA = forearc, AA = arc axis, RA = rear-arc.

[d] Non-primitive lava.

[e] Lava with trace element abundances and radiogenic isotope ratios suggestive of source mixing or mixing between CAB and HAOT.

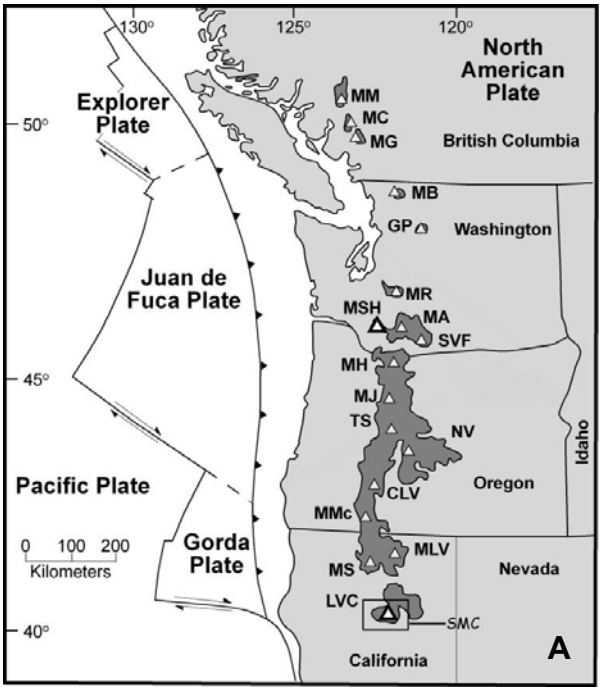
130°
125°
120°
50°
45°
40°
North American Plate
Explorer Plate
Juan de Fuca Plate
Pacific Plate
Gorda Plate
British Columbia
Washington
Oregon
Nevada
California
Idaho
MM
MC
MG
MB
GP
MR
MSH
MA
SVF
MH
MJ
TS
NV
CLV
MMc
MLV
MS
LVC
SMC
0 100 200
Kilometers
A

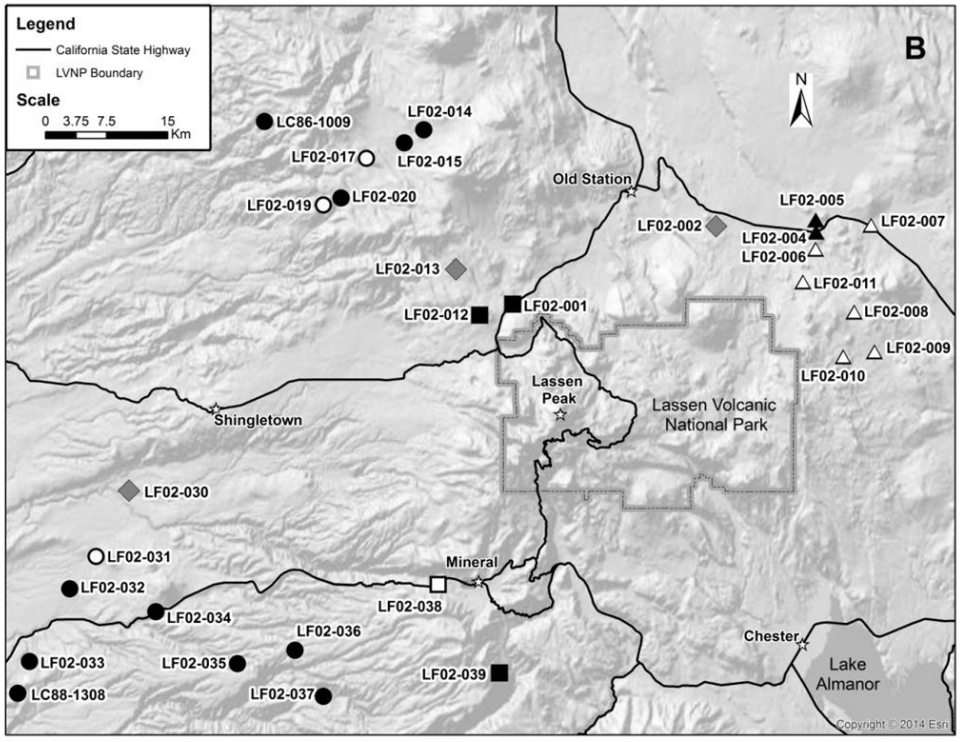
Legend
California State Highway
LVNP Boundary
Scale
0 3.75 7.5 15
Km
B
N
LC86-1009
LF02-014
LF02-017
LF02-015
Old Station
LF02-019
LF02-020
LF02-005
LF02-002
LF02-007
LF02-004
LF02-006
LF02-013
LF02-011
LF02-012
LF02-001
LF02-008
LF02-009
LF02-010
Lassen Peak
Lassen Volcanic National Park
Shingletown
LF02-030
LF02-031
Mineral
LF02-032
LF02-038
LF02-034
LF02-036
Chester
LF02-033
LF02-035
LF02-039
Lake Almanor
LC88-1308
LF02-037
Copyright © 2014 Esri

FIGURE 1

This is a preprint, the final version is subject to change, of the American Mineralogist (MSA)
Cite as Authors (Year) Title. American Mineralogist, in press.
(DOI will not work until issue is live.) DOI: http://dx.doi.org/10.2138/am-2016-5588CCBY

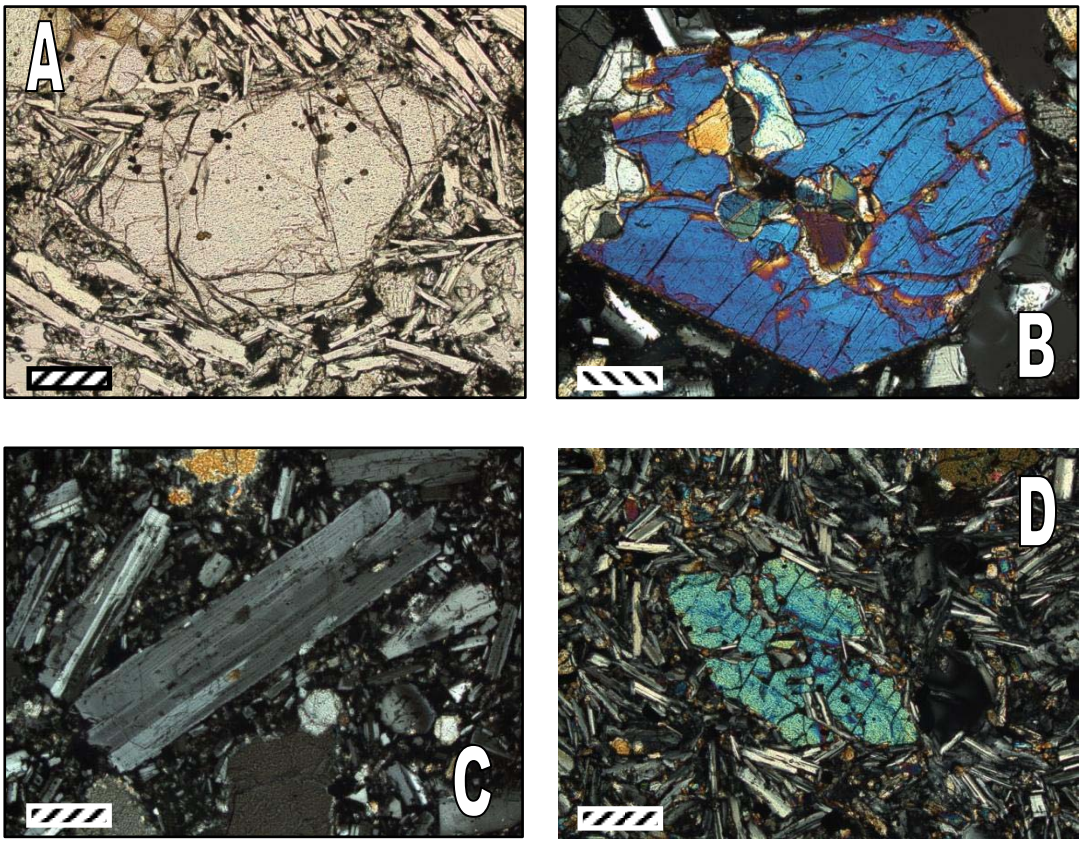

FIGURE 2

This is a preprint, the final version is subject to change, of the American Mineralogist (MSA)
Cite as Authors (Year) Title. American Mineralogist, in press.
(DOI will not work until issue is live.) DOI: http://dx.doi.org/10.2138/am-2016-5588CCBY

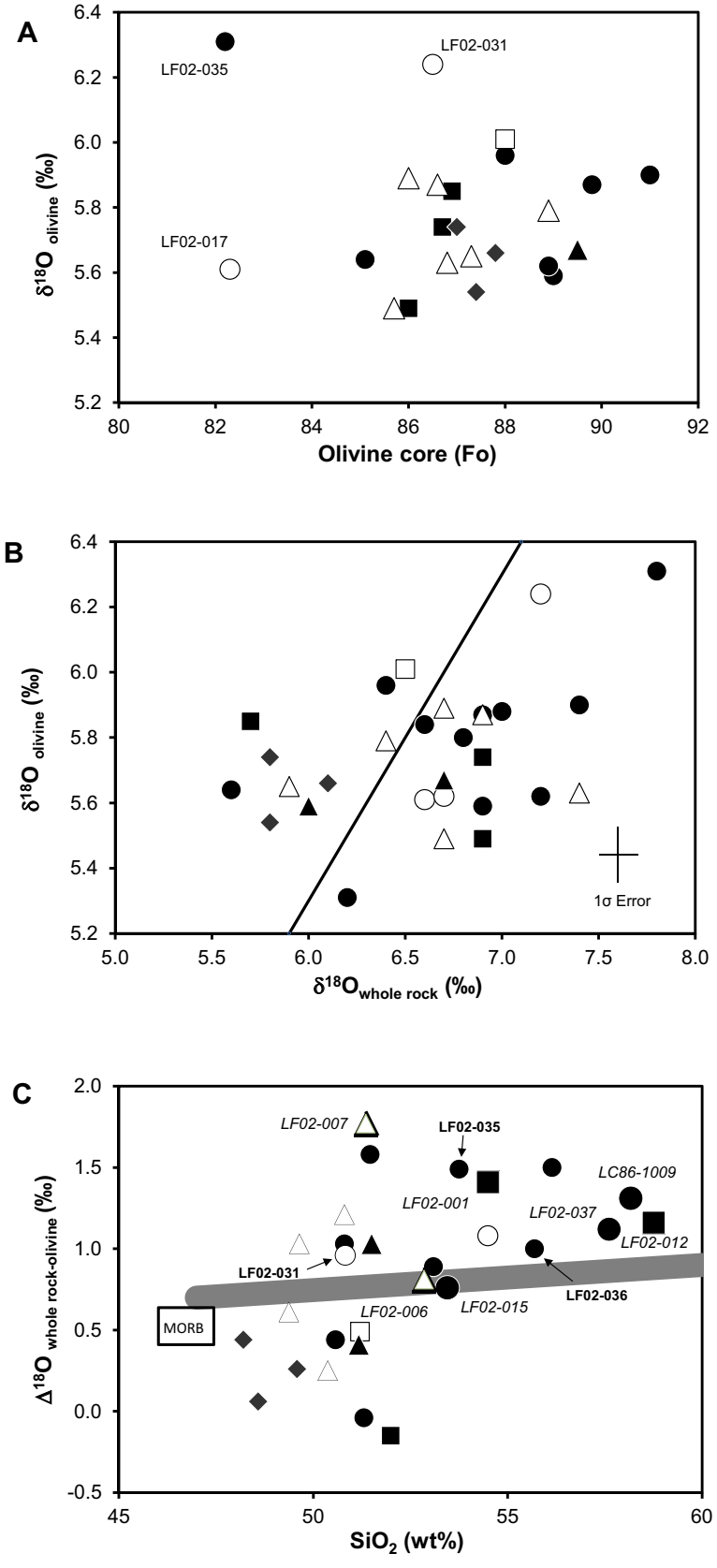

Figure 3

This is a preprint, the final version is subject to change, of the American Mineralogist (MSA)
Cite as Authors (Year) Title. American Mineralogist, in press.
(DOI will not work until issue is live.) DOI: http://dx.doi.org/10.2138/am-2016-5588CCBY

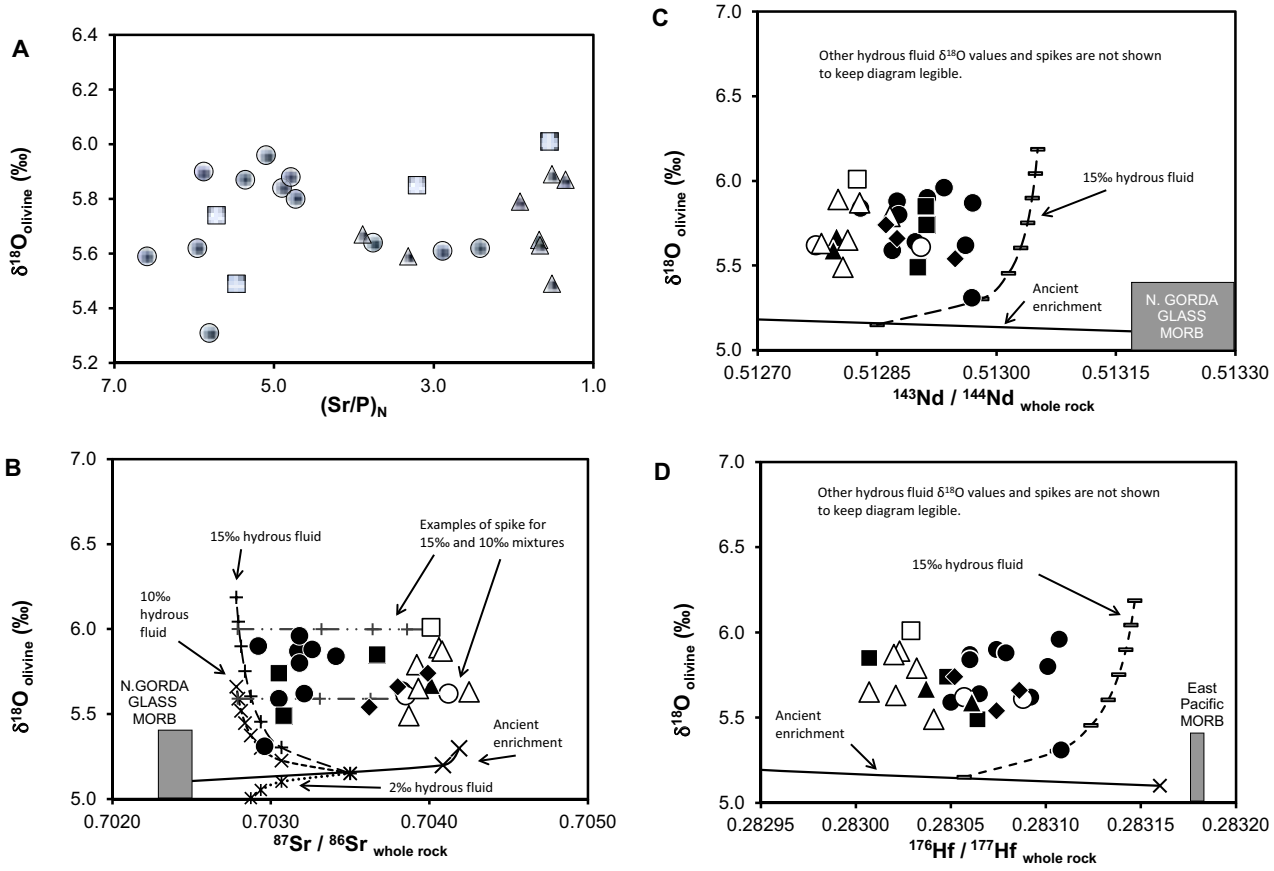

Figure 4

This is a preprint, the final version is subject to change, of the American Mineralogist (MSA)
Cite as Authors (Year) Title. American Mineralogist, in press.
(DOI will not work until issue is live.) DOI: http://dx.doi.org/10.2138/am-2016-5588CCBY

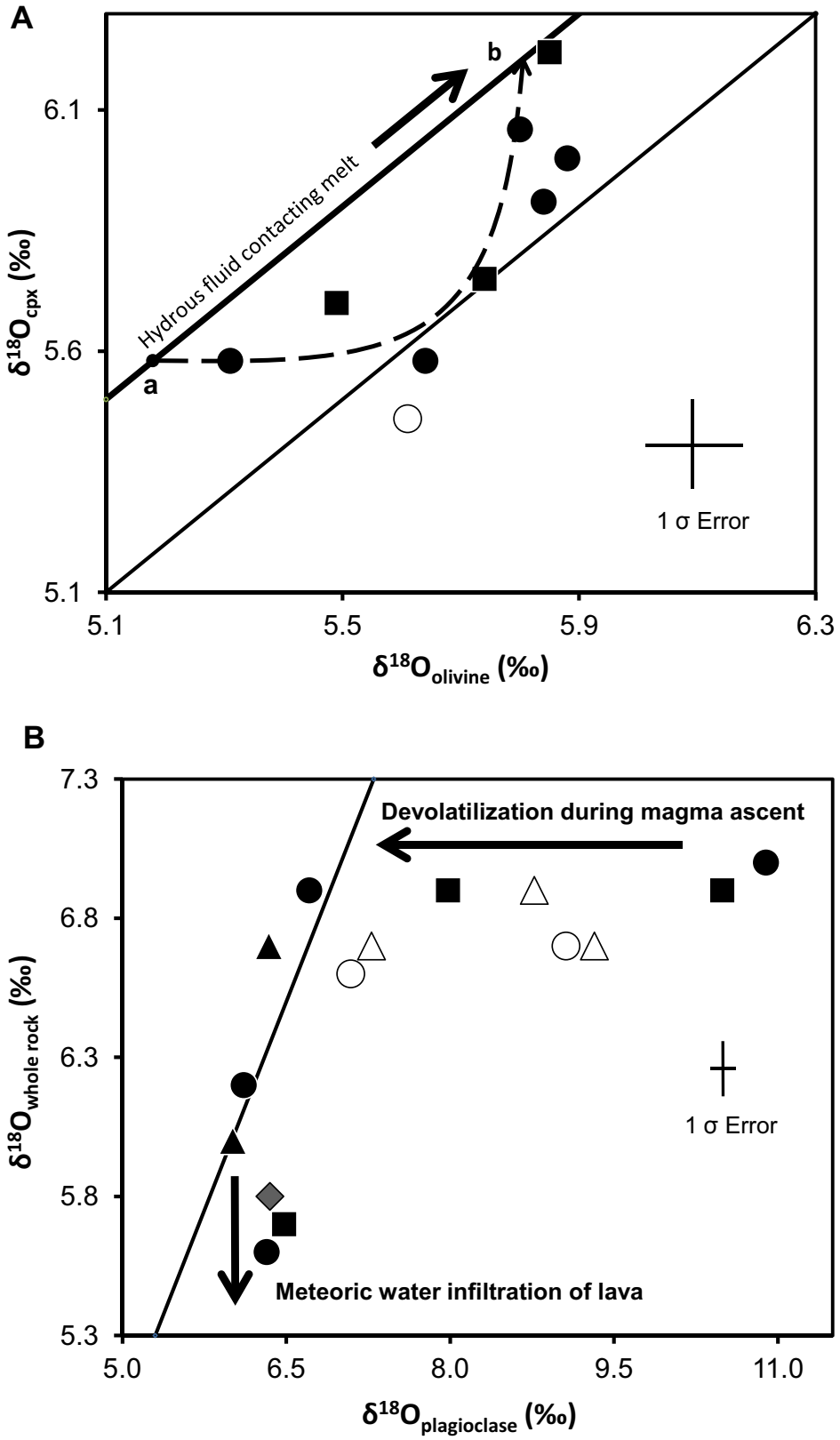

Figure 5

This is a preprint, the final version is subject to change, of the American Mineralogist (MSA)
Cite as Authors (Year) Title. American Mineralogist, in press.
(DOI will not work until issue is live.) DOI: http://dx.doi.org/10.2138/am-2016-5588CCBY

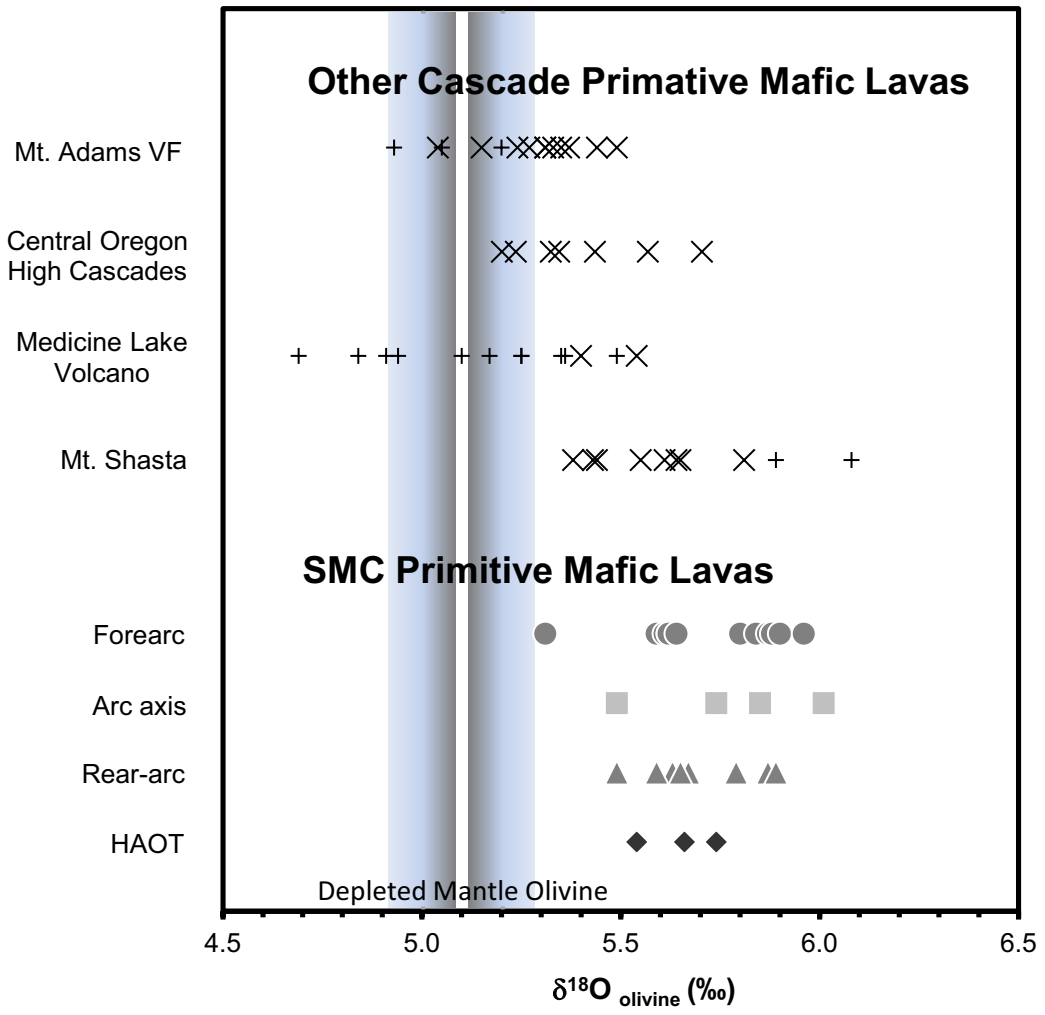

Figure 6